Bulgarian Chemical Communications, Volume 50 Special Issue A (pp. 13-21) 2018

Comparative electrochemical and topographical elucidation of Anodic Aluminum Oxide (AAO) layers formed on technically pure aluminum (TPA) and AA2024-T3 aircraft alloy

S. V. Kozhukharov*, Ch. A. Girginov

University of Chemical Technology and Metallurgy, 8 St. Kliment Ohridski blvd. 1756 Sofia, Bulgaria

Received June 28, 2017; Accepted October 07, 2017

The remarkable difference between the mechanical properties of pure aluminum and its industrial alloys predetermines significant variations in their chemical comportment. This fact imposes more detailed investigations on the correlation between the alloy's chemical composition and its behavior during the preliminary chemical treatments and further exposure to corrosive media. In this sense, the present research is devoted to the comparison of Anodic Aluminum Oxide (AAO) films, formed at the same conditions on technically pure aluminum (TPA) and the highly doped (AA2024-T3) aircraft alloy. The anodization process was performed galvanostatically with simultaneous in-situ chrono-potentiometric curve recording. The electrochemical behavior of the investigated anodized specimens in 3.5 %NaCl medium was elucidated by Electrochemical Impedance Spectroscopy (EIS) and Linear Voltammetry (LVA). The topology of the obtained AAO films was observed by Scanning Electron Microscopy (SEM) and Atomic Force Microscopy (AFM). Remarkable differences between the AAO films formed on TPA and AA2024-T3 were registered by all analytical techniques used in the present research. The electrochemical methods used have shown completely different curve shapes and the further numerical analysis confirmed the observed significant dissimilarities. The SEM and AFM surface observations also revealed entirely different surface morphologies, for both investigated aluminum compositions. The remarkably distinguishable morphologies were observed in both cases: prior to and after anodization. Summarizing the results of both types of electrochemical measurements and the topological observations, it can be inferred that the TPA forms uniform barrier AAO film, whereas the oxide layer on AA2024-T3 is rather cracked and possesses lower durability in the model corrosive medium.

Keywords: Aluminum anodization, AA2024-T3, EIS, LVA, SEM, AFM

INTRODUCTION

Although the anodization process has been intensively studied [1-13] and well described in the literature [14], its impact on Al-based industrial alloys is not sufficiently investigated. On the other hand, the industrial branch requires highly doped alloys with extended mechanical strength and reliable exploitation characteristics [15, 16]. The alloying dopants promote chemical and structural heterogeneity, which enhances the resulting alloys' susceptibility to localized corrosion [17-22]. Especially, the Cu-Mg-doped AA2024 type of alloys contains a large variety of intermetallic inclusions, which precipitate during the finishing metallurgical thermal post-treatments [23, 24]. These inclusions initiate considerable deviations of the alloy surface behavior from the expected for pure aluminum. In a previous work [25], it was established that the AA2024-T3 alloy has different behavior than a clad alloy with the same composition, during both coating primer deposition and subsequent corrosion tests. In addition, only a few papers on the AA2024-T3 anodization were found [26-28], but the results reported in these works are not compared to pure aluminum.

All these facts have predetermined the aim of the present research: to compare the electrochemical characteristics and topological features of Anodized Aluminum Oxide (AAO) films, obtained at the same conditions on technically pure aluminum and AA2024-T3 aircraft alloy.

EXPERIMENTAL

Two sets by three samples of (Al 99.5%) technically pure aluminum (signed as TPA) and AA2024-T3 were submitted to anodization, followed by subsequent electrochemical measurements and morphological observations. Prior to anodizing, all samples underwent preliminary treatment by etching in 50 g dm^{-3} NaOH solution at 60 °C and activation in diluted HNO_3 (1:1 v/v) at room temperature. Both procedures were performed for two minute, followed by vigorous cleaning with tap and distilled water.

The anodization was performed at galvanostatic (15 mA cm^{-2}) and isothermal (20 °C)

* To whom all correspondence should be sent.
E-mail: stephko1980@abv.bg

conditions for 48 minutes with simultaneous in-situ chrono-potentiometric curves acquisition. The curve recording enabled to determine the AAO formation voltage (U_f) with anodization time (t). A two electrode cell, with 250 ml of 15%wt. of H_2SO_4 with continuous stirring was used. The zones submitted to anodization were circular with 24.5 mm diameter for all samples.

The electrochemical measurements were performed after 24 and 168 hours of exposure to 100 ml 3.5% NaCl model corrosive medium in three electrode cells. The exposed areas from the anodized zones were 16 mm in diameter and served as working electrodes. This lower surface area was selected, in order to avoid any edge effects. The signal acquisition was performed against Ag/AgCl/3M KCl reference electrode and cylindrical platinum mesh, serving as a counter electrode.

The measurements were performed using Electrochemical Impedance spectroscopy (EIS), followed by Linear Voltammetry (LVA) in cathodic and anodic directions. The former was performed from 10 kHz to 10 mHz, with 50 frequency steps at 20 to 120 mV, according to the Open Circuit Potential (OCP). This relatively high excitation signal amplitude interval was selected because of the high oxide layer resistance (corresponding to definitely insulating properties in the case of pure aluminum). After each EIS spectrum acquisition, individual cathodic (from 30 to -500 mV) and anodic (from -30 to 500 mV) LVA curves were acquired, respectively. The anodic curves were recorded at least 3 hours after the respective cathodic ones, in order to restore the initial OCP values. The potential sweep in both cases was 10 mVs^{-1}, in order to avoid any significant polarization and electrode damage.

The AAO morphology of some of the samples was additively observed by Scanning Electron Microscopy (SEM), using a TESCAN SEM/FIB LYRA I XMU device. The respective Atomic Force Microscopy (AFM) observations were performed on both cases of technically pure aluminum and AA2024-T3 alloy. These observations were done in dynamic regime by Eayscan 2, "Nanosurf" (Switzerland) on square zones with linear size of 49.5 μm from both the anodized and bare areas, at 256 points per line of resolution. The AFM device was equipped by TAP 190-G cantilever, produced by Budgetsensors (Bulgaria).

RESULTS AND DISCUSSION

In-situ data acquisition

In general terms, all the curves look quite similar, being composed of a sharp vertical slope at the beginning and horizontal line until the end of the anodization process (Fig. 1).

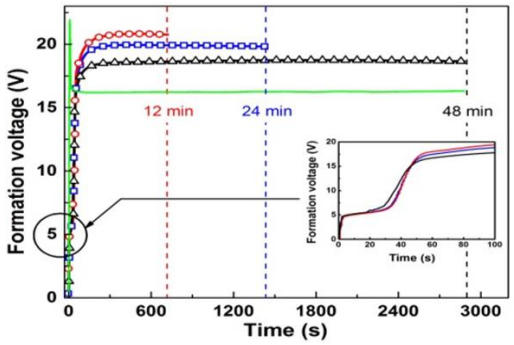

Fig. 1. In-situ chronopotentiometric curves, acquired during the anodization process

However, the more detailed analysis of the $U_f(t)$-curves reveals a sharp initial rise (until 22.5 V) in the case of TPA, whereas for AA2024-T3 alloy, there is a retention at about 30 - 40 s at 5 V. This fact is related to the differences in the initial oxide layers, formed on Al-foil and AA2024-T3 alloy during the preliminary treatment procedures. In the former case, the oxide layer is more uniform and has specific resistance of 1.5 kΩ cm^2, whereas in the latter case the potential barrier at 5 Volts is somehow related to the thinner oxide layer, corresponding to a resistance of about 0.3 kΩ cm^2. The occurrence of the potential retention at 5 V is related either to copper oxidation or oxide layer growth on the Al matrix adjacent and beneath the intermetallic inclusions, after their dissolution.

Another difference between the in-situ $U_f(t)$-curves is that the horizontal part in the case of TPA is situated at 16.3 V, whereas the curves of the AA2024-T3 alloy are positioned at 18.75 V. This difference is related to the larger specific surface area provided by the alloy. It is a consequence of the higher roughness (commented in the next sections), resulting from the intermetallics' selective dissolution, during both the preliminary treatment procedures and the anodization process itself. Finally, it is worth mentioning that the horizontal parts of the chrono-potentiometric curves correspond to gradual proceeding of Al-oxidation conjugated with reduction of H_3O^+ ions to H_2 on the cathode. In the case of AA2024-T3, these processes are coincided with metallic Cu deposition on the counter electrode. Thus, in the case of AA2024-T3, besides reactions 1 and 3, additional reactions 2 and 4 proceed:

On the anode:

$$4Al^0 + 18H_2O \rightarrow Al^{3+} + Al_2O_3 + 6H_3O^+ + 6e^- \quad (1)$$

$$Cu^0 \rightarrow Cu^{2+} + 2e^- \quad (2)$$

On the cathode:

$$6H_3O^+ + 6e- \rightarrow 6H_2O + 3H_2 \quad (3)$$

$$Cu^{2+} + 2e^- \rightarrow Cu^0 \quad (4)$$

The additional reactions (2 and 4) require higher voltage, in order to achieve 15 mA cm^{-2}, which is the reason for the higher U_f values for the alloy.

Electrochemical measurements

The already anodized TPA and AA2024-T3 samples were submitted to systematical electrochemical measurements during exposure to 3.5% NaCl model corrosive medium. These measurements were performed by two electrochemical analytical methods.

Electrochemical Impedance Spectroscopy

The impedance spectra acquired at the initial 24 hours of exposure were not sufficiently representative, probably due to intensive adsorption and penetration of the corrosive medium species across the oxide layers. Well-ordered impedance spectra were acquired after 168 hours of exposure. As it was mentioned in the experimental section, the TPA samples needed EIS data acquisition at much higher amplitudes (120 mV versus OCP), in order to obtain readable spectra.

The rather distinguishable shapes of the EIS spectra for the investigated types of aluminum reveal clear structural differences of the AAO film properties, as consequence of the respective substrate compositions. An example of typical EIS spectra acquired for both the investigated compositions (i.e. TPA and AA2024) is represented in Fig. 2.

The dependence of the phase shift (φ) on the excitation signal frequency (f) (i.e. $\varphi(f)$- curves) for TPA show almost completely pure capacitance from 1 kHz to 10 mHz, tending to 90° angular. For comparison, the respective curves for AA2024-T3 in the Bode plots (position b) show two maxima at the high and middle frequency ranges, combined with indistinguishable inflexion at the lowest frequencies.

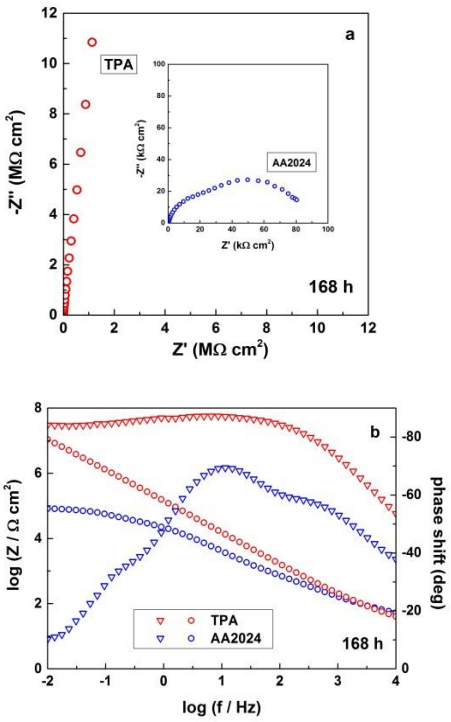

Fig.2. EIS spectra for AAO films after 168 hours of exposure to the model corrosive medium

The Nyquist plots recorded for both types of samples look rather different, as well. In the former case (TPA) almost vertical arcs are obtained, whereas in the alloy case, overlapped semi-circles are observable. It is noteworthy, that pure capacitors give vertical lines and consequently the pure aluminum AAO films behave as almost pure capacitors. Such behavior can be explained assuming dense dielectric film, formed on TPA. Another reason for the occurrence of almost completely pure capacitance might be the higher surface smoothness in the case of the technically pure aluminum.

The rather different spectra shapes required different equivalent circuits (EC) for quantitative data fitting analysis (Fig. 3).

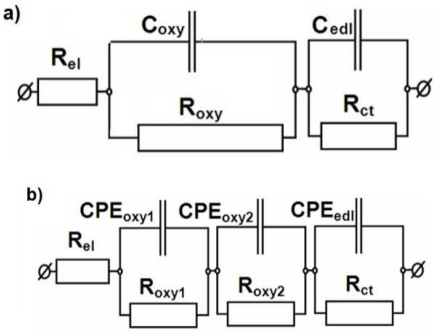

Fig. 3. Equivalent circuits used for EIS data fitting: (a) technically pure Al (TPA) and (b) AA2024-T3 aircraft alloy

The spectra acquired for TPA are composed by only two time constants (i.e. parallel RC units), whereas the data for AA2024-T3 were successfully fitted to circuits, composed by three time constants, connected in series.

Another, rather interesting feature of the equivalent circuit, appropriate for the pure Al spectra fitting was that the use of capacitors (C) was more suitable instead of constant phase elements (CPEs). This fact is an additional evidence for the purely capacitive behavior of the AAO films in this case.

The necessity for description of the AAO formed on the AA2024-T3 alloys by surface CPEs reveals structural and topological irregularity of the oxide layer in this case. This irregularity is an obvious consequence of the variation of the oxide layer growth kinetics on the intermetallic inclusion locations and the basic alloys' Al-matrix. During the anodization process, copper deposition was observed on the cathode, according to reaction (4). This fact is an evidence for Cu-dissolution from the AA 2024-T3 alloy (reaction 2), coinciding the AAO growth. Initially, it was suggested, that the occurrence of two time constants in the case of AA2024-T3 is a result of the simultaneous AAO growth on the basic Al-matrix (with higher rate) and under the actively dissolving Cu-intermetallics (with lower rate, hindered by reactions 2 and 4). However, this assumption is not consistent, because otherwise the oxide layer time constants (CPE_{oxy1} R_{oxy1}) and (CPE_{oxy2} R_{oxy2}) should be connected in parallel, but the data fitting to such equivalent circuit was not successful. The consecutive connection of both time constants reveals occurrence of an interface inside the oxide layer. Thus, distinguishable exterior and interior AAO composing layers are obviously formed. The outer electrolyte/outer oxide interface (CPE_{oxy1}) and the resistance (R_{oxy1}) of the electrolyte penetrated in its defects belong to the upper irregular film. Beneath this outer layer, another, inner layer is formed with a well-defined intermediate interface. This interphase is characterized by its own constant phase element (CPE_{oxy2}) and ohmic resistance (R_{oxy2}). This resistance is probably related to electrolyte penetration towards the metallic surface or Al^{3+} ion transport resistance, as proposed in [1].

The last time constant for both equivalent circuits (C_{edl} or CPE_{edl} and R_{ct}) is related to the chemical reactions of the corrosion process (i.e. oxygen reduction and Al-oxidation) of the already formed AAO films.

In order to evaluate the data dissipation, the numerical data of all the investigated samples obtained by the data fitting of the EIS the spectra by the equivalent circuits (Fig 3) are summarized in Table 1.

The R_{ct} value of sample 3 of TPA group has shown 96.85% deviation. The same trend has been shown by the rest pure aluminum samples after larger exposure times. Probably, the equivalent circuit undergoes changes, due to corrosion product accumulation.

Linear voltammetry

The averaged LVA curves in Fig. 4, acquired after 168 hours of exposure show even more remarkable differences between the typical behavior possessed by the AAO layers on TPA and the alloy, respectively. The LVA results confirm the statements done for the EIS spectra. Indeed, both the cathodic (position a) and anodic (position b) types of curves show significant differences.

The cathodic curves for TPA are almost horizontal, due to the barrier passivation of AAO film, whereas the curves acquired for the AA2024-T3 alloy are smooth and reveal clear occurrence of corrosion processes, being positioned at much higher current densities.

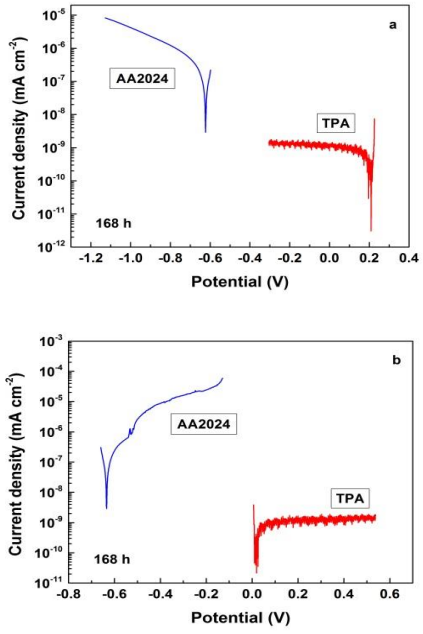

Fig. 4. Cathodic (a) and anodic (b) polarization curves acquired after 168 hour of exposure of the investigated specimens.

Similar trends are observable for the respective anodic curves. Besides, the anodic curves of the alloy possess inflexions, revealing localized corrosion activities [34]. The registered current densities for TPA approach the equipment detection minimum threshold, due to the strong insulating properties of its AAO film.

All differences between the curves' shapes described above evince the aptitude of TPA to form dense and uniform AAO with well-expressed barrier properties, whereas the AA2024-T3 forms an oxide layer which does not protect the alloy efficiently.

The LVA curves, acquired after 168 hours of exposure for all investigated samples were submitted to further Tafel slope analysis and the results are shown in Table 2.

The corrosion potential (E_{corr}) values of the alloy samples are in a very narrow interval between -618 and -634 mV, (measured vs. Ag/AgCl/3M KCl), whereas a great E_{corr} dissipation was registered for the pure aluminum. The mentioned E_{corr} deviations for TPA are a result of the insignificant current densities (approaching the equipment detection minimum threshold). The R_p values for TPA are by two orders of magnitude higher than those for AA2024-T3. This fact is an additional evidence for the superior barrier properties of the AAO, formed on the technically pure aluminum.

Table1. EIS data fitting results from the spectra acquired after 168 hours of exposure

Anodized TPA samples					
Element	Unit		Sample **1**	Sample **2**	Sample **3**
R_{el}	$\Omega\ cm^2$		28.24 ± 3.08	50.74 ± 6.78	50.04 ± 4.90
C_{oxy}	$\mu F\ cm^{-2}$		1.50 ± 0.12	0.760 ± 0.10	1.40 ± 1.40
R_{oxy}	$\Omega\ cm^2$	10^3	1.568 ± 0.76	0.29 ± 0.06	3.08 ± 0.80
C_{edl}	$\mu F\ cm^{-2}$		0.685 ± 0.01	0.570 ± 0.01	0.70 ± 0.01
R_{ct}	$\Omega\ cm^2$	10^6	102.80 ± 28.26	120.40 ± 38.44	286.40 ± 274.54
Anodized AA2024-T3 alloy					
Element	Unit		Sample **1**	Sample **2**	Sample **3**
R_{el}	$\Omega\ cm^2$		16.04 ± 0.73	40.38 ± 2.85	14.42 ± 0.76
Q_{oxy1}	$s^n\Omega^{-1}cm^{-2}$	10^{-6}	4.23 ± 0.49	27.78 ± 6.00	48.04 ± 1.84
n	-		0.88 ± 0.03	1.00 ± 0.09	0.96 ± 0.02
R_{oxy1}	$\Omega\ cm^2$	10^3	0.85 ± 0.13	51.78 ± 12.32	12.16 ± 1.34
Q_{oxy2}	$s^n\Omega^{-1}cm^{-2}$	10^{-6}	7.78 ± 0.51	4.31 ± 0.19	7.30 ± 1.22
n	-		0.77 ± 0.01	1.00 ± 0.03	0.95 ± 0.04
R_{oxy2}	$\Omega\ cm^2$	10^3	71.00 ± 15.14	31.50 ± 5.05	0.48 ± 0.06
Q_{edl}	$s^n\Omega^{-1}cm^{-2}$	10^{-6}	14.78 ± 2.50	19.62 ± 3.10	27.25 ± 2.28
n	-		0.96 ± 0.03	0.60 ± 0.15	0.65 ± 0.07
R_{ct}	$\Omega\ cm^2$	10^3	161.00 ± 16.09	109.60 ± 14.61	40.80 ± 1.08

Table 2. Tafel plot analysis of the polarization curves acquired after 168 hours of exposure

	Cathodic curves R_p ($k\Omega\ cm^2$)		Anodic curves R_p ($k\Omega\ cm^2$)	
Sample	**TPA**	**AA 2024**	**TPA**	**AA 2024**
S 1	$22.90x10^3$	192.08	$26.76x10^3$	192.26
S 2	$23.32x10^3$	161.90	$40.14x10^3$	157.30
S 3	$51.10x10^3$	41.72	$37.60x10^3$	45.90

The corrosion potential (E_{corr}) values of the alloy samples are in a very narrow interval between -618 and -634 mV, (measured vs. Ag/AgCl/3M KCl), whereas a great E_{corr} dissipation was registered for the pure aluminum. The mentioned E_{corr} deviations for TPA are a result of the insignificant current densities (approaching the equipment detection minimum threshold). The R_p values for TPA are by two orders of magnitude higher than those for AA2024-T3. This fact is an additional evidence for the superior barrier properties of the AAO, formed on the technically pure aluminum.

Impact of the anodization process on the surface morphology

Scanning Electron Microscopy

The SEM images (Fig. 5) reveal that the impact of the anodization process for the technically pure aluminum and the highly doped

AA2024-T3 differs. In the former case, the AAO film repeats the substrate's topology. It can be described as laminar surface (inset of position (a)) with multitude of pits (position (a) basic image). The laminar surface is obtained during the Al-foil rolling, whereas the pits are formed during the preliminary etching and acid activation.

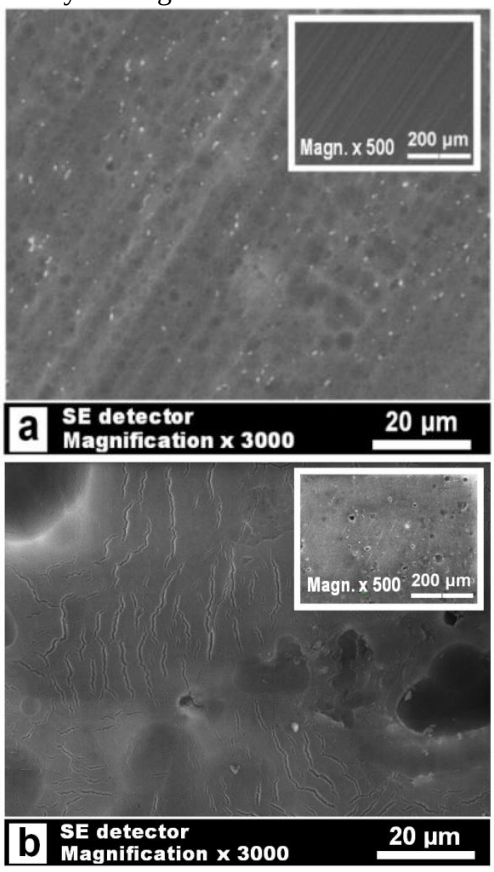

Fig. 5. SEM images of the investigated samples: (a) TPA and (b) AA2024-T3

The AAO layer, formed on AA2024-T3 is covered by multitude of cracks and ruptures. In addition, in the inset of position (b) a large number of wide caverns (not pits) are observable. The results of previous research works dedicated on the preliminary treatment of this alloy [31-33] lead to the inference that these concavities are rather result of the sample etching and acidic activation than to be consequence of the anodization process. These observations completely correlate with the EIS data analysis results. Probably, the cracks and ruptures, together with the entrapped electrolyte correspond to (CPE_{oxy1} R_{oxy1}), whereas the time constant (CPE_{oxy2} R_{oxy2}) shows that these defects do not reach the metallic surface, hence a denser inner oxide layer is present.

Atomic Force Microscopy

The AFM images (Fig. 6) reveal that in the case of TPA, the AAO film repeats the substrate's topology. Consequently, the anodization of the technically pure aluminum results in only slight smoothening of the laminas and increase of the pits' number and depth.

For comparison, the AA2024-T3 surface looks rather different from the above described even prior to anodization. Besides the cracks commented above (regarding the SEM images), wide caverns instead of pits are observable for the alloy samples. Also, coarse formations are observable, probably due to occurrence of large-sized intermetallics, which are formed during the thermal treatment of the alloy.

The formation of pits and caverns during the preliminary treatments (etching and acidic activation) can be ascribed to selective dissolution phenomena. These phenomena involve the smaller grains in the case of TPA and adjacent Al-matrix surrounding the cathodic intermetallics of the AA2024-T3 alloy, respectively.

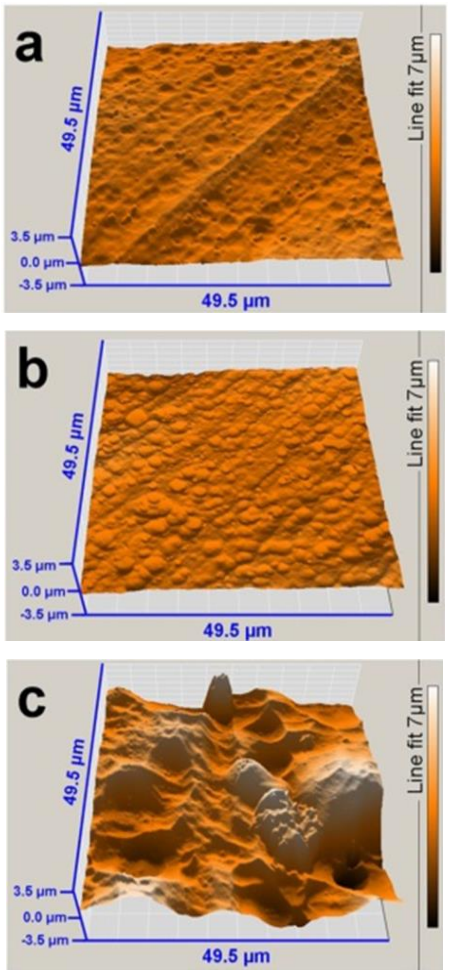

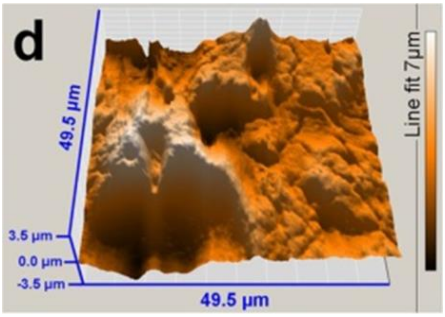

Fig. 6. AFM images of reference (a, c) and anodized (b, d) samples of TPA (a, b) and AA2024-T3 (c, d)

The quantitative AFM data analysis for TPA causes surface roughness increment, regarding the roughness mean (S_m) from 0.4 to 31.2 pm. This S_m increase (of almost 80 times) confirms the inference for pit depth and number increase during the anodization.

For comparison, the anodization of AA2024 leads to greater topological changes than in the case of TPA. The AAO film formed on the alloy shows that the anodization results in twice rougher topology (S_m values from 62.8 pm for TPA up to 190.1 pm for AA2024). This difference can be explained, considering the coincidence of Al-oxide film growth and selective dissolution around the intermetallics.

The maximal distance between the highest and the lowest points (S_y) for TPA changes from S_y = 1.50 to 1.31 µm, due to the anodization process. This S_y decrement with about 0.30 µm is consequence of the smoothening of the laminar ridges, which cannot be compensated by the pitting proliferation, discussed above. For comparison, the AA2024-T3 samples preserve their topology with negligible decrease of S_y from 6.40 to 6.14 µm, regarding the total roughness.

CONCLUSIONS

The in-situ chronopotentiometric curves of TPA possess a sharp initial rise (until 22.5 V), whereas for AA2024-T3 alloy, there is retention of about 30-40 s at 5 V. This phenomenon is related to the differences of the initial oxide layers, formed on TPA foil and AA2024-T3 alloy during the preliminary treatment procedures. The occurrence of the potential retention at 5 V is probably related either to Cu-intermetallics oxidation, or to adjacent Al matrix oxide layer growth, coinciding the intermetallics dissolution. Besides, the horizontal parts of TPA are slightly lower, compared to those for the alloy. This fact is a result of the higher roughness, resulting from the intermetallics selective dissolution during the preliminary treatment procedures.

The TPA samples needed EIS data acquisition at a much higher excitation signal amplitude, in order to obtain readable spectra. The rather distinguishable EIS spectra shapes for the pure aluminum and the alloy reveal clear structural differences of the AAO films, as consequence of the respective substrate compositions. These rather different spectra shapes required different equivalent circuits for quantitative data fitting analysis. The analysis results have shown purely capacitive properties of the AAO formed on TPA, whereas the alloy showed irregular oxide layer, due to intermetallic occurrence.

The cathodic curves for TPA are almost horizontal, due to the barrier passivation of AAO film, whereas the respective curves acquired for the AA2024-T3 alloy are smooth and reveal clear occurrence of corrosion processes. Similar trends are observable for the respective anodic curves. Besides, the anodic curves of the alloy possess inflexions, revealing localized corrosion activity. The polarization resistance (R_p) values for TPA are by two orders of magnitude higher than those for AA2024-T3, because of the superior barrier properties of the AAO, formed on the technically pure aluminum. The corrosion potential (E_{corr}) values of the alloy samples are in a very narrow interval, but a great E_{corr} dissipation was registered for TPA as a result of the random pit distribution, as well as the insignificant current densities, near to the equipment detection minimum threshold.

The SEM and AFM images reveal that the impact of the anodization process for the technically pure Al and the highly doped AA2024-T3 is quite different. In the former case, the anodization results in only slight smoothening of the laminas and increase of the pits' number and depth. The AA2024-T3 surface looks rather different from the above described even prior to anodization. Wide caverns instead of pits are observable for the alloy samples. Besides, coarse formations are also observable, probably due to occurrence of large size intermetallics, which are formed during the thermal treatment of the alloy. The formation of pits and caverns during the preliminary treatments can be ascribed to selective dissolution of smaller grains of the TPA, and adjacent Al-matrix surrounding the cathodic intermetallics of the AA2024-T3 alloy, respectively. Its AAO film has a more distinguishable topology, compared to the respective bare alloy. The quantitative AFM data analysis shows that the AAO film is twice smoother for TPA, than the bare AA2024-T3 alloy (with S_m values of 190.10 to 62.8 pm), because of

coincidence of Al-oxide film growth and selective dissolution.

Summarizing the results of the electrochemical measurements and the topological observations, it can be inferred that the TPA forms uniform AAO, whereas the oxide layer on AA2024-T3 is composed by a cracked outer layer and an underlayer.

***Acknowledgements**: The funding of this work under contract DFNI-T02–27 by the Bulgarian National Scientific Research Fund is highly appreciated.*

REFERENCES

1. J. Siejka, C. Orteg, *J. Electrochem. Soc*. **124**, 883 (1977).
2. V.P. Parkhutik, J. M. Albella, Yu. E. Makushok, I. Montero, J.M. Martinez-Duart, V.I. Shershulskii, *Electrochim. Acta*, **35**, 955 (1990).
3. V.P. Parkhutik, V.T. Belov, M.A. Chernyckh, *Electrochim. Acta*, **35**, 961 (1990).
4. Ch. Girginov, S. Kozhukharov, *Internat. J. Electrochem.* (2011), Article ID 126726; doi:10.4061/2011/126726
5. V. Surganov. C. Jansson. J.G. Nielsen. P. Morgen, *Electrochim. Acta*, **33**, 517 (1988).
6. K.V. Heber, Electrochim. Acta 23, 127 (1978).
7. K.V. Heber, *Electrochim. Acta*, **23**, 135 (1978).
8. F. Nasirpouri, M. Abdollahzadeh, M.J. Almasi, N. Parvini-Ahmadi, *Current Appl. Phys.*, **9**, S91 (2009).
9. A. Bai, C-C.Hu, Y-F.Yang, C-C. Lin, *Electrochim. Acta*, **53**, 2258 (2008).
10. C-U. Yu, C-C.Hu, A. Bai, Y-F. Yang, *Surf. Coat. Tech.*, **201**, 7259 (2007).
11. J.M. Montero-Moreno, M. Sarret, C. Müller, *Surf. Coat. Tech.*, **201**, 6352 (2007).
12. S. Ono, M. Saito, H. Asoh, *Electrochim. Acta*, **51**, 827 (2005).
13. M. Ghorbani, F. Nasirpour , A. Iraji-zad, A. Saedi, *Materials & Design*, **27**, 983 (2006).
14. W. J. Stępniowski, M. Salerno, Chapter 12. Fabrication of nanowires and nanotubes by anodic alumina template-assisted electrodeposition, Manufacturing Nanostructures (Eds. Waqar Ahmed, Nasar Ali), One Central Press (2014) pp. 321-357.
15. E. A. Starke, Jr., J. T. Staley, Prog. Aerospace Sci., 32, 131 (1996).
16. S. V. Kozhukharov, Deposition of Environmentally Compliant Cerium-Containing Coatings and Primers on Copper-Containing Aluminium Aircraft Alloys, Biobased and Environmental Benign Coatings (eds A. Tiwari, A. Galanis and M. D. Soucek), John Wiley & Sons, Inc. (2016), Hoboken, NJ, USA. p. 20
17. F.M. Queiroz, M. Magnani, I. Costa, H.G. de Melo, *Corr. Sci.*, **50**, 2646 (2008).
18. Ch. Blanc, G. Mankowski, *Corr. Sci*., **40**, 411 (1998).
19. J.A. DeRose, T. Suter, A. Bałkowiec, J. Michalski, K.J. Kurzydlowski, P. Schmutz, *Corr. Sci.*, **55**, 313 (2012).
20. A. Aballe, M. Bethencourt, FJ. Botana, M. Marcos, M.A. Rodríguez-Chacón, *Rev. Metal.*, **34**, 42 (1998).
21. V. Guillaumin, G. Mankowski, *Corr. Sci*. **41**, 421 (1998).
22. A. Boag, R.J. Taylor, T.H. Muster, N. Goodman, D. McCulloch, C. Ryan, B. Rout, D. Jamieson, A.E. Hughes, *Corr. Sci*., **52**, 90 (2010).
23. A. E. Hughes, C. MacRae, N. Wilson, A. Torpy, H. T. Muster, A. M. Glenn, Surf. *Int. Anal.*, **42**, 334 (2010).
24. C. Blanc, B. Lavelle, G. Mankowski, *Corr. Sci.*, **39**, 495 (1997).
25. S. Kozhukharov, M. Milanes, C. Girginov, M. Machkova, *Materials and Corrosion*, DOI: 10.1002/maco.201508635
26. M. Zaki-Mubarok, W. Sutarno, S. Wahyudi, *J. Min. Mater. Char. Eng*., **3**, 154 (2015).
27. G. Boisier, N. Pébère,a, C. Druez, M. Villatte, S. Suelb, *J. Electrochem. Soc*., **155**, C521 (2008).
28. M. Xiangfeng, W. Guoying, G. Hongliang, Y. Yundan, C. Ying, H. Dettinger, *Int. J. Electrochem. Sci.*, **8**, 10660 (2013).
29. S. Kozhukharov, Ch. Girginov, I. Avramov, M. Machkova, *Mat. Chem. Phys.*, **180**, 301 (2016).
30. M. Curioni, P. Skeldon, E. Koroleva, G. E. Thompson, J. Ferguson, *J. Electrochem. Soc.*, **156**, C147 (2009).
31. E. A. Matter, S. Kozhukharov, M. Machkova, V. Kozhukharov, *J. Chem. Tech. Metall*., **50**, 52 (2015).
32. E. A. Matter, S. V. Kozhukharov, M. S. Machkova, *Bul. Chem. Comm.*, **43**, 23 (2011).
33. E. Matter, S. Kozhukharov, *Ann. proceed. Univ. Rousse (Bulgaria),* **49**, 14 (2010).
34. M. Bethencourt, F.J. Botana, J.J. Calvino, M. Marcos, M.A. Rodriguez-Chacon, *Corr. Sci.*, **40**, 1803 (1998).

СРАВНИТЕЛНО ЕЛЕКТРОХИМИЧНО И ТОПОЛОГИЧНО ИЗСЛЕДВАНЕ НА АНОДНИ ОКСИДНИ ФИЛМИ ФОРМИРАНИ ВЪРХУ ТЕХНИЧЕСКИ ЧИСТ АЛУМИНИЙ И САМОЛЕТНА AA2024-T3 СПЛАВ

С. В. Кожухаров, К. А. Гиргинов

Химикотехнологичен и металургичен университет, бул. Климент Охридски № 8, 1756 София (България)

Постъпила на 28 юни 2017 г.; приета на 07 октомври 2017 г.

(Резюме)

Големите разлики в механичните свойства на чистия алуминий и неговите индустриални сплави предопределя значителни вариации на тяхното химично и електрохимично поведение. Този факт налага по-подробно изследване на връзката между състава на сплавта и нейното отнасяне при предварителните химични обработки, както и при излагане в корозионни среди. Настоящото изследване е посветено на сравнението на анодните оксидни филми (AAO), формирани при еднакви условия върху технически алуминий (TPA) и високо легирана сплав (AA2024-T3). Анодирането е провеждано в галваностатично-изотермичен режим, като са регистрирани in-situ хроно-потенциометрични кинетични криви. Електрохимичното поведение на анодираните образци в 3.5% NaCl среда е изследвано чрез електрохимична импедансна спектроскопия (EIS) и линейна волтаметрия (LVA). Топологията на формираните AAO филми е наблюдавана чрез сканираща електронна микроскопия (SEM) и атомно-силова микроскопия (AFM). Чрез използваните аналитични техники е установена забележима разлика в отнасянията на AAO-филмите, образувани върху TPA и тези върху AA2024-T3. Използваните електрохимични методи показаха напълно различни отнасяния, което е потвърдено и от извършения допълнителният цифров анализ на експерименталните данни. Повърхностните наблюдения (SEM и AFM) разкриха напълно различна топологична картина на повърхността за двата изследвани алуминиеви състава. От обобщението на резултатите от електрохимичните измервания и топологичните наблюдения, може да се заключи, че TPA образува равномерен AAO филм, докато оксидният слой върху AA2024-T3 е по-скоро напукан и притежава по-малка трайност в моделната корозивна среда.

Ключови думи: анодиране на алуминий, AA2024-T3, EIS, LVA, SEM, AFM